Local Models for Oil Well Casing Subject to Subsidence Deformations

Emílio C. C. M. Silva[1]

[1]*Well Engineering, Petrobras*
R. do Senado, 115, 16º andar, Centro, 20231-003, Rio de Janeiro/RJ, Brazil
emiliosilva@petrobras.com.br

Abstract. When oil and gas wells become depleted and reservoir pressures decreases, the porous formation contracts due to poromechanics effects, causing significant stress redistribution and global deformation of the rock mass, up to the surface, a phenomenon called subsidence. Both surface and underground displacements are transmitted to well barrier elements, including wellheads, casing and cementing, potentially leading to hydrocarbon leaks. However, coupling geomechanical models of subsidence with well structures presents significant modeling and simulation challenges. Axisymmetric modeling of vertical wells subject to transversely isotropic subsidence strains is relatively straightforward and extensible to slightly deviated wells, but any other scenario requires costly and challenging tridimensional modeling. Therefore, although subsidence is a global problem, it is important to develop local coupling models. In this work, we present a contracting material model for the rock, which allowed us to isolate the casing loads induced by generalized strain states. We demonstrate how these results can be interpreted as traditional loads used in well casing design approach.

Keywords: well casing design, subsidence, well integrity.

1 Introduction

Subsidence is a general term for the vertical displacements of the earth surface, including the bottom of water bodies, caused by geomechanical phenomena. In the oil and gas industry, relevant subsidence occurs when high porosity reservoirs are severely depleted, due to the compaction of the reservoir and general stress redistribution, leading to a global displacement field that becomes apparent as subsidence [1]. Tectonics, such as fault reactivation, can also cause significant strains [2], and may therefore be studied with similar techniques.

The structure of oil and gas wells is anchored to the rock at several places, from the conductor casing to the cemented segment of the production casing. In open hole completion, the production string may be directly anchored to the formation through open hole packers or gravel pack material. Even when not cemented, casing and tubing are still bound to the borehole by friction forces. The strains imposed by the formation can lead to loss of cement hydraulic isolation and mechanical failure of structural elements. If critical well barrier elements are damaged, formation fluids can flow to the surface or to aquifers.

These hydrocarbon leaks can be hard to detect and costly to fix, therefore it is important to prevent the damage to operating and abandoned wells by proper simulation of geomechanical loading [3]. If strains are moderate, it is feasible to account for subsidence during well design, preparing the structure for the additional loads. This can be done using well structure models and geomechanical models of subsidence. Vertical wells with axisymmetric loads can be simulated using axisymmetric models [4]. Other scenarios, including deviated and horizontal wells, as well as severe shear loads, requires costly and challenging tridimensional modeling [3], [5], [6].

2 Modeling

For demonstration of the proposed methodology, we use a cylindrical 3D solid model composed of two parts, representing an empty 9 ⅞″ 66.9 ppf casing (outer radius 0.12541 m, inner radius 0.10845 m), inserted in a rock domain, 10 m long, with a 10 m radius (see Figure 1). We focus the analysis on the central section, which we consider representative of the local behavior of a well cross-section. To simplify the interpretation of the results, there is no cement sheath. Table 1 summarizes the model parameters.

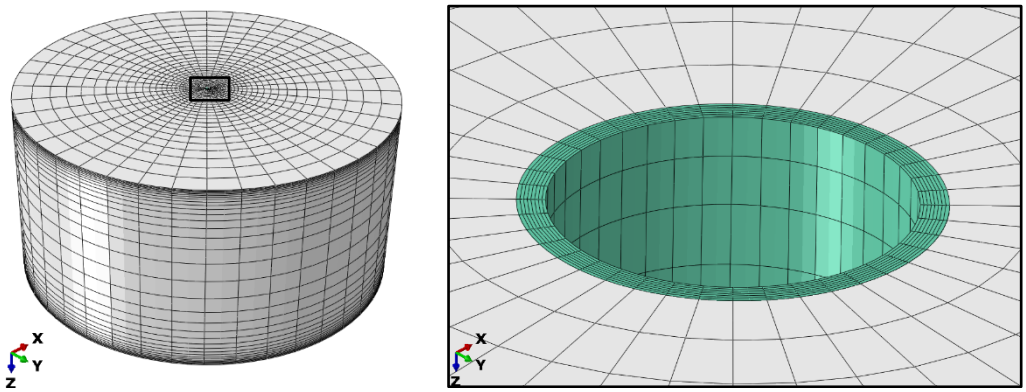

(a) Rock domain (b) Casing domain (dark) embedded in the rock (light)

Figure 1. Illustration of rock and casing domains and meshes.

Table 1. Geometric parameters and material properties

Parameter	Value	Units
Outer rock radius	10	m
Inner rock radius	0,12541	m
Outer casing radius	0,12541	m
Inner casing radius	0,10845	m
Length	10	m
Elastic modulus – rock	40	GPa
Poisson coefficient – rock	0.2	–
Elastic modulus – casing	206.843	GPa
Poisson coefficient – casing	0.3	–
Yield stress – casing	758.42	MPa

We used Dassault's Abaqus [7] finite element analysis package to perform the numerical simulations. The system was discretized with a finite element mesh of 20-node hexahedral elements with quadratic displacement interpolation, hybrid formulation and reduced integration (C3D20RH). Bonding between rock and casing was enforced with `*TIE` constraints, which do not allow any relative slip. Casing and rock are linear elastic. Rigid body motion is constrained by distributed coupling to a fixed reference point. Besides the application of swell creep strain, there are no other loads and no additional displacement boundary conditions in the examples below.

2.1 Global to local model coupling

We assume that the presence of the well does not disturb the global displacement field of the rock, therefore we will use the rock strains as the boundary conditions of our local model. The simplest coupling between the geomechanical model and the local submodel, specially in a displacement-based numerical formulation, is to match displacements at the interface, imposing a local displacement field that is consistent with the strains obtained from the global model.

In this paper, we propose a novel coupling strategy, in which we impose the global strain to the rock as an imposed creep strain. As the casing resists to this strain, coupling stresses arise between it and the rock, while the system stays fully self-equilibrated. This feature allows us to prepare the model as desired, including *in situ* stresses, hydrostatic fluid and cement pressures and initial casing loads, ensuring that subsidence strains are added independently of those initial and boundary conditions.

In the simulation, anisotropic swelling creep (which can also model contraction) was prescribed on the rock using the `*SWELLING` keyword and the `*RATIOS` modifier, which allows prescribing different swell ratios to three orthogonal directions. We ran the model in a `*VISCO` time step for one time unit, during which the desired strain was reached. We found that implementing this strategy is straightforward and that the method is flexible enough to allow for heterogeneous deformation fields, using field variables to vary the strain rate spatially.

2.2 Coordinate systems

In the text, three coordinate systems are used. Global coordinates of the geomechanics simulation are indicated by the indices *x, y, z*, where $\vec{e}_z$ is the vertical direction (with gravity pointing to the negative side), $\vec{e}_x$ is the east-west direction, pointing to the east, and $\vec{e}_y$ is the north-south direction, pointing to the north. Wellbore coordinates are represented by *u, v, s*, where $\vec{e}_s$ is the direction of the well, pointing toward the wellhead ($\vec{e}_z$ for a vertical well), $\vec{e}_u$ is the high side of the cross section (or $\vec{e}_x$ for a vertical well) and $\vec{e}_v$ is the lateral side (perpendicular to $\vec{e}_u$ and $\vec{e}_s$). Finally, the principal directions of the global strain tensor are represented as $\vec{e}_1$, $\vec{e}_2$ and $\vec{e}_3$. Compressive strains are negative, and the principal strains are ordered as $E_{11} \geq E_{22} \geq E_{33}$. The wellbore directions can be obtained from directional information (inclination θ and azimuth ϕ) using Eqs. (3) to (5):

$$\vec{e}_s = \begin{bmatrix} \sin\theta\cos\phi \\ \sin\theta\sin\phi \\ -\cos\theta \end{bmatrix}, \tag{1}$$

$$\vec{e}_u = \begin{cases} \dfrac{\vec{e}_z - (\vec{e}_z \cdot \vec{e}_s)\vec{e}_s}{\|\vec{e}_z - (\vec{e}_z \cdot \vec{e}_s)\vec{e}_s\|}, & \text{if } |\vec{e}_z \cdot \vec{e}_s| \neq 1 \\ \vec{e}_x, & \text{if } |\vec{e}_z \cdot \vec{e}_s| = 1 \end{cases} \tag{2}$$

$$\vec{e}_v = \vec{e}_s \times \vec{e}_u. \tag{3}$$

2.3 General strain state

For the general case, we assemble the parts (rock and casing) in the well coordinate system and rotate them to the global coordinate system at the assembly level. Material orientations are relative to the part, therefore we first rotate the strain state $\mathbf{E}^{xyz}$ to this system using a rotation matrix $\mathbf{R}$:

$$\mathbf{R} = [\vec{e}_u \quad \vec{e}_v \quad \vec{e}_s] = \begin{bmatrix} e_{ux} & e_{vx} & e_{sx} \\ e_{uy} & e_{vy} & e_{sy} \\ e_{uz} & e_{vz} & e_{sz} \end{bmatrix}, \tag{4}$$

$$\mathbf{E}^{uvs} = \mathbf{R}^{\mathrm{T}}\mathbf{E}^{xyz}\mathbf{R}. \tag{5}$$

We then find the principal strains (E_{11}, E_{22} and E_{33}) and principal directions ($\vec{e}_1$, $\vec{e}_2$ and $\vec{e}_3$) in this base. Since Abaqus cannot apply shear strains with the `*SWELLING` keyword, we assign these principal strain directions to the material orientation of the rock. We then use the `*RATIOS` keyword to apply the three principal strains.

3 Results

3.1 Axial strain loading

To deform the casing of a vertical in the axial direction, the system was loaded with uniform strain of 0.001 in the *z* direction. Figure 2 shows that the displacements and strains are progressively communicated through shear stresses at the rock-casing interface at the outer boundaries. Away from the boundaries, the system deforms uniformly in plane strain conditions. The stress state is the same as that of ordinary axial loading. If slippage is allowed between rock and casing, the shear stress is limited by the shear strength of the interface. In this case, the strain transfer region will be longer.

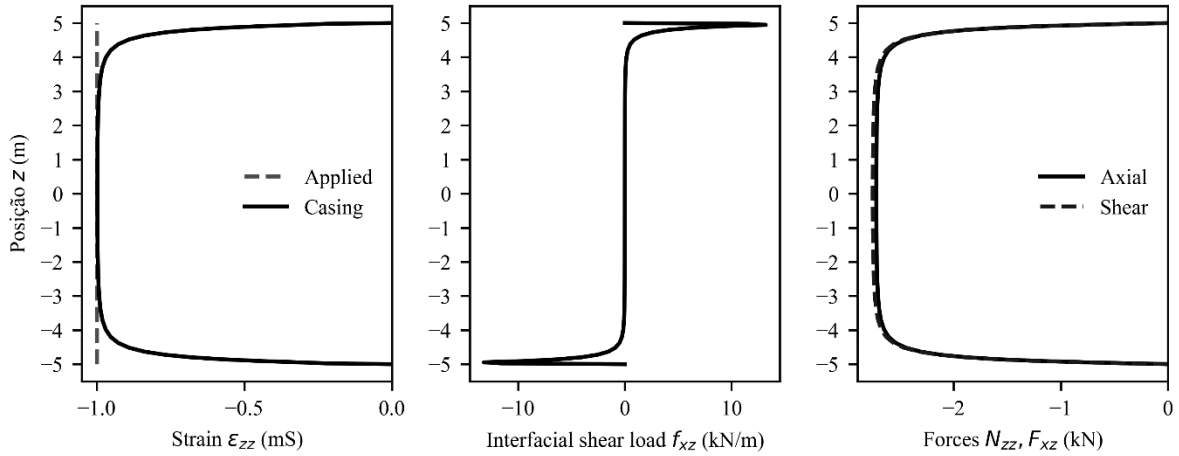

(a) Casing axial strain (b) Casing–rock interaction (c) Sectional forces

Figure 2. Effects of pure axial subsidence on casing: (a) Axial strains applied on the rock and measured in the casing section; (b) Shear force applied by the rock on the casing, by unit length; (c) Axial force in the casing and accumulated shear force acting in the casing.

Casing failure in compression can be delayed significantly if buckling is restrained [8]. Progressive yielding will permanently shorten the casing, as observed in the field [9], and increase its thickness. Actual loss of structural integrity will depend on the behavior of the connections. On the other hand, cement failure and loss of zonal isolation in the annulus should be expected.

3.2 Transverse strain loading

In order to simulate a horizontal well section subject to subsidence loads, we applied a uniform strain of 0.001 in the *x* direction, perpendicular to the casing. For simplicity, we did not rotate the casing itself. Figure 3(a) shows that the magnitude of the strain is not fully transmitted to the casing. The highest compressive strains appear on the sides, ninety degrees from the loading direction, and there are no significant strains in the other directions.

The casing is ovalized by the applied strain, similarly to non-uniform salt loading [10]. We note that the whole system is approximately in plane strain conditions, with stresses mainly in the circumferential direction, around the inner diameter (Figure 3b). These stresses can be added directly to those generated by external pressure loads, reducing the collapse strength of the pipe. No significant boundary effects were observed at the pipe ends.

The main observable effect of ovalization is difficulty in operating tools inside the well. In severe cases, damage to the production or injection tubing string can occur, including control lines and data cable.

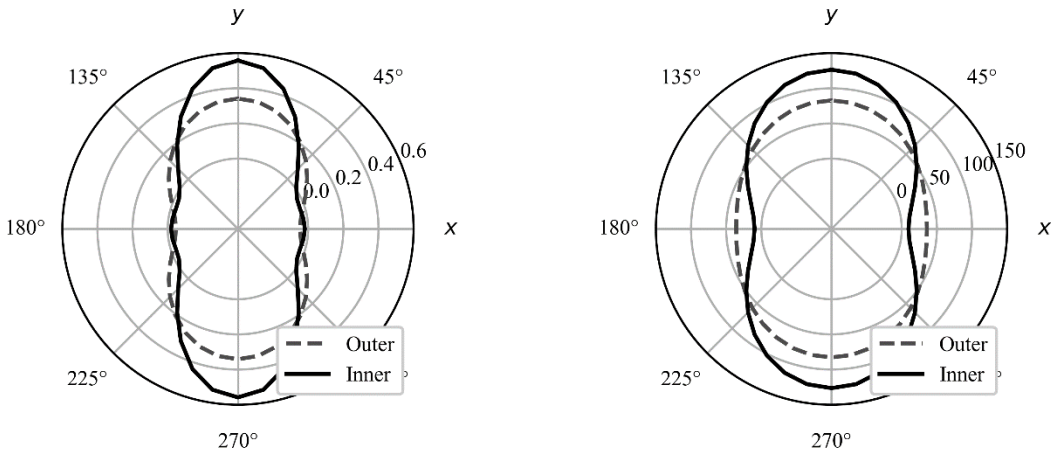

(a) Strain ε_{xx} (compressive, mS) (b) Circumferential stress (compressive, MPa)

Figure 3. Effects of subsidence in the *x* direction, perpendicular to casing: (a) Strains ε_{xx} at the inner and outer casing surfaces; (b) Circumferential stresses at the inner and outer casing surfaces.

3.3 Pure shear loading

Pure shear conditions (i.e. no volume change) are not expected in a subsidence model. However, it is instructive to consider the effects of shear separately from axial and transverse loading, especially since this scenario cannot be modeled in 2D plane strain conditions. We applied a pure shear $\varepsilon_{xz} = 0.005$ to the model. Figure 4 shows that some equivalent stress is induced by shear, albeit lower than the in the other loading cases.

Nevertheless, shear strains on the casing do occur naturally, either as a result of vertical deformation acting on an inclined well, or also at shallow shear regions around the reservoir border [11]. Shear failures are observed in the field as casing ovalization and cross-sectional fracture [12].

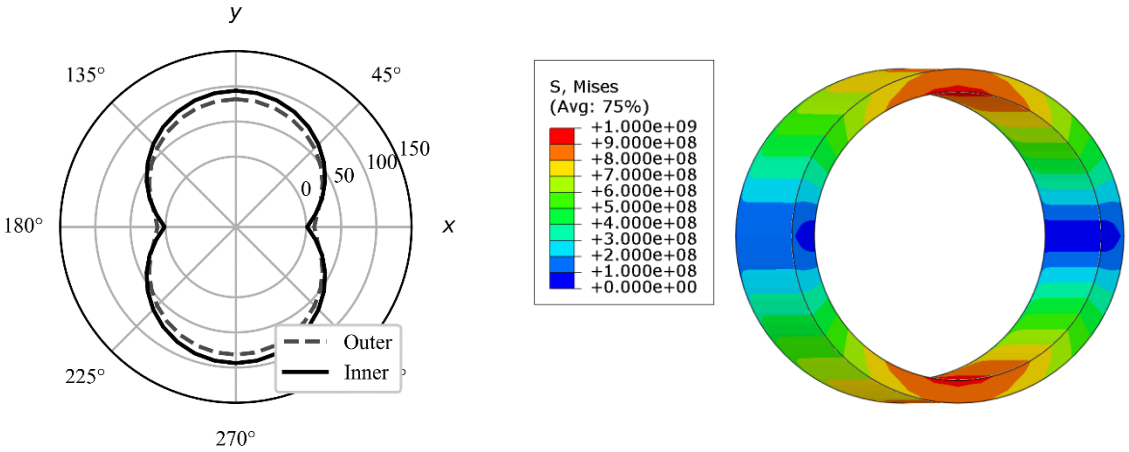

(a) Von Mises equivalent stress σ_m (MPa) (b) Von Mises equivalent stress σ_m (Pa)

Figure 4. Effects of pure shear strain loading in the *xz* plane: (a) Von Mises equivalent stress σ_m at the inner and outer casing surfaces; (b) Contour lines of σ_m in the deformed configuration, viewed from the *z* direction.

3.4 Application in well casing design

In the elastic domain, we can model the loading on a specific cross section as a superposition of these three kinds of subsidence loads and the traditional design loads. We propose an interpretation of the subsidence results

as a reduction in the API design envelope. For pure axial strain loading, the stress state is equivalent to an axial force, which reduces the axial compressive. For the case examined in Section 3.1, the maximum load is -2.723 kN (-612.2 kips). The effects on the design envelope of the casing (Figure 3a) are illustrated in Figure 3(b).

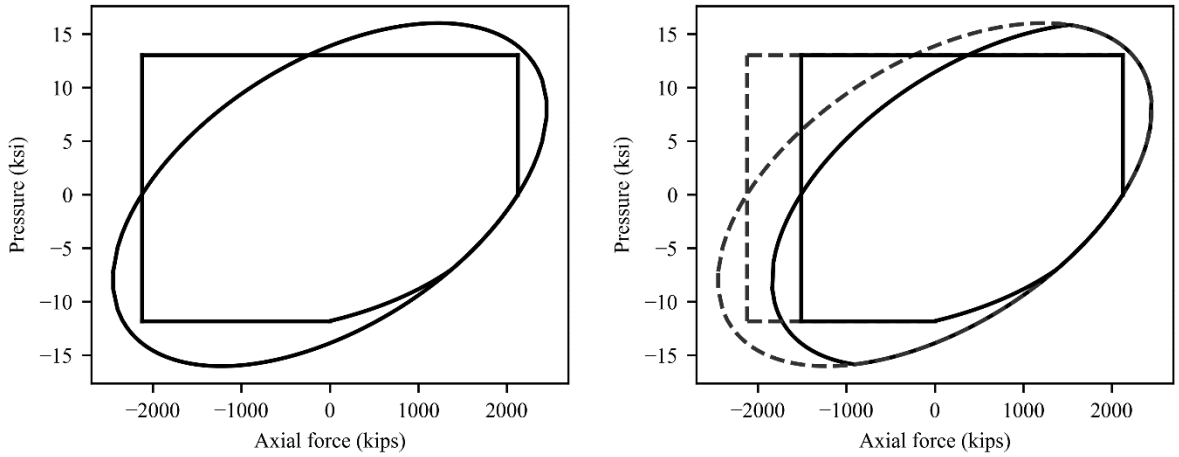

(a) API casing design envelope (b) Design envelope with axial subsidence strain

Figure 5. Effects of axial subsidence strains on the design envelope: (a) API design envelope of 9 ⅞″ 66.9 ppf 110 ksi casing; (b) Reduced design envelope after axial strain $\varepsilon_{ss} = 0.001$.

The transverse strain case (Section 3.2) displays hoop stresses analogous to those produced by external pressure. Since both loads induce maximal hoop stresses at the casing ID, we can treat the transverse strain as a fictitious external pressure, similar to the treatment of bending stresses in API TR 5C3 [13]. For the case in study, the peak stress is -126.5 MPa (-18340 psi). Using Lame's equations, we find an equivalent pressure of 2314 psi. The resulting design envelope is shown in Figure 6(a).

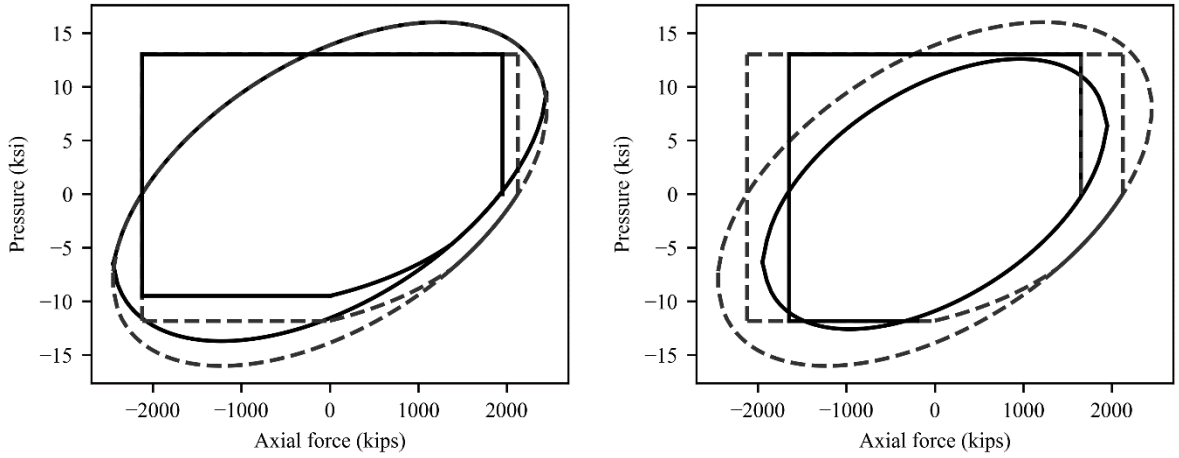

(a) Design envelope with transverse strain (b) Design envelope with shear strain

Figure 6. Effects of subsidence strains on the API design envelope: (a) Reduced design envelope after transverse strain $\varepsilon_{uu} = 0.001$.; (b) Reduced design envelope after shear strain $\varepsilon_{us} = 0.005$.

Finally, the shear strain case (3.3) has no analogue in either force or pressure, but the maximum shear occurs in the same plane and direction as the shear created by torsion, so it can enter as τ_{ha} in the von Mises equivalent stress formula

$$\sigma_e = (\sigma_r^2 + \sigma_h^2 + \sigma_a^2 - \sigma_r\sigma_h - \sigma_r\sigma_a - \sigma_h\sigma_a + 3\tau_{ha}^2)^{1/2}, \quad (6)$$

where σ_r is the radial stress from actual internal and external pressures, σ_h is the hoop stress from actual pressures and the fictitious subsidence pressure, σ_a is the axial stress from axial loads, bending and axial subsidence strain, and τ_{ha} is the shear stress due to both torsion and shear subsidence strain. Figure 6(b) shows the resulting design envelope.

4 Conclusions

We presented a methodology to apply subsidence strain loads obtained from global geomechanical models to local models of cemented casing. The method can be used to apply general triaxial strain states to critical section of wells in any orientation, reproducing the unusual loading patterns associated with reservoir compaction. The resulting stress states can be interpreted as traditional design loads, shrinking the design envelope of the pipe.

Acknowledgements. The authors acknowledge the valuable discussions and contributions of Petrobras' Research Center and Well Engineering divisions, especially Rafael Dias, Nelson Moreira Jr., Charlton Souza, Ricardo Pioli, as well as Asset Engineer Flávia Falcão.

Authorship statement. The authors hereby confirm that they are the sole liable persons responsible for the authorship of this work, and that all material that has been herein included as part of the present paper is either the property (and authorship) of the authors, or has the permission of the owners to be included here.

References

[1] M. S. Bruno, "Geomechanical Analysis and Decision Analysis for Mitigating Compaction Related Casing Damage," p. 13.

[2] A. . Casero and M. . Rylance, "The Unconventional Unconventionals: Tectonically Influenced Regions, Stress States and Casing Failures," in *February 06, 2020*, The Woodlands, Texas, USA: SPE, Jan. 2020, p. SPE-199710-MS. doi: 10.2118/199710-MS.

[3] S. French *et al.*, "4-D Geomechanics to Predict Compaction and Subsidence for Development of Unconsolidated Sandstone Reservoirs: Fortuna Project Case Study, Offshore Equatorial Guinea," in *Day 3 Thu, March 16, 2017*, The Hague, The Netherlands: SPE, Mar. 2017, p. D031S013R006. doi: 10.2118/184603-MS.

[4] I. A. Pimentel, J. V. Uribe, D. D. de Melo, S. A. Fontoura, and L. M. Almeida, "Casing Integrity Evaluation in Oil Wells Submitted to Subsidence Loads," presented at the 55th U.S. Rock Mechanics/Geomechanics Symposium, Jun. 2021, p. ARMA-2021-1985.

[5] P. M. T. M. Schutjens *et al.*, "Compaction- and Shear-Induced Well Deformation in Tyra: Geomechanics for Impact on Production," *Rock Mech Rock Eng*, vol. 52, no. 12, pp. 5205–5224, Dec. 2019, doi: 10.1007/s00603-019-01892-8.

[6] X. Shen and R. Pounds, "Numerical Analysis on the 3D Mechanical Behavior of Completion Tubing under Subsidence Loading," in *All Days*, Kuala Lumpur, Malaysia: IPTC, Dec. 2014, p. IPTC-17764-MS. doi: 10.2523/IPTC-17764-MS.

[7] Dassault Systèmes, *Abaqus 2022 Documentation*. in SIMULIA User Assistance. Paris, France, 2023. Accessed: Apr. 29, 2023. [Online]. Available: https://help.3ds.com/

[8] N. Morita and S. Shiozawa, "Stability Analysis of Casings During Plastic Deformation," in *Day 1 Wed, September 10, 2014*, Galveston, Texas, USA: SPE, Sep. 2014, p. SPE-170303-MS. doi: 10.2118/170303-MS.

[9] A. Yudovich, L. Y. Chin, and D. R. Morgan, "Casing Deformation in Ekofisk," *Journal of Petroleum Technology*, vol. 41, no. 07, pp. 729–734, Jul. 1989, doi: 10.2118/17856-PA.

[10] F. L. G. Pereira, M. De Simone, and D. Roehl, "Wellbore Integrity Assessment Considering Casing-Cement-Formation Interaction Based on a Probabilistic Approach," presented at the 51st U.S. Rock Mechanics/Geomechanics Symposium, Jun. 2017, p. ARMA-2017-0164.

[11] G. H. Schwall and C. A. Denney, "Subsidence Induced Casing Deformation Mechanisms in the Ekofisk Field," in *All Days*, Delft, Netherlands: SPE, Aug. 1994, p. SPE-28091-MS. doi: 10.2118/28091-MS.

[12] B. A. Dale, G. M. Narahara, and R. M. Stevens, "Case History of Reservoir Subsidence and Wellbore Damage Management in the South Belridge Diatomite Field," *SPE Production & Facilities*, vol. 15, no. 01, pp. 50–57, Feb. 2000, doi: 10.2118/60844-PA.

[13] API, "API TR 5C3 Calculating Performance Properties of Pipe Used as Casing or Tubing," American Petroleum Institute, 2018.